TECHNICAL PROGRESS REPORT 386
NOTS TP 3736
COPY 88

FABRY-PEROT TYPE LASER MODULATORS

by

Donald G. McCauley
Test Department

ABSTRACT. This report describes the optical characteristics of two prototype laser modulators having the thin, flat, disk-shaped Fabry-Perot (F-P) interferometer design. The modulators are being used to investigate the use of laser radiation in communications. The report discusses the intensity modulation resulting both from the converse-piezoelectrically-induced oscillations in the physical separation of the interferometer reflectors and from the electrooptically-induced oscillations in the optical separation of the interierometer reflectors.

Other Test Department reports prepared to date on laser investigations include TPR 356, Fluorescence Pumping of Lasers; TPR 376, Fluorescence Pumping of Lasers: Experiments With Coaxial Xenon Flash Tube; and TPR 377, GaAs Injection Laser Investigation (in preparation).

45-50

U.S. NAVAL ORDNANCE TEST STATION

China Lake, California

April 1965

U. S. NAVAL ORDNANCE TEST STATION

AN ACTIVITY OF THE BUREAU OF NAVAL WEAPONS

J. I. HARDY, CAPT., USN
Commander

WM. B. McLEAN, PH.D.
Technical Director

FOREWORD

This is one in a series of progress reports to be published on investigations being conducted at NOTS on laser techniques and applications. It is a partial product of an extended program begun in the Research Department Semiconductor Physics Branch and presently in progress in the Photophysics Branch of the Test Department. The program is designed to explore many of the arguments for using laser radiation in communications. Two light modulators having the Fabry-Perot interferometer design are reviewed. The classical parameters controlling the reflected and transmitted intensities from this type interferometer are related to the carrier wave modulation frequency and depth, both of which concepts are vital to communications.

The work was done during the period July 1963 through July 1964 and was supported by exploratory and foundational research funds.

Released by
F. M. ASHBROOK, Head
Instrument Development Division
2 November 1964

Under authority of
WM. B. McLEAN
Technical Director

NOTS Technical Publication 3736
Technical Progress Report 386

Published by	Test Department
Manuscript	30/MS-685
Collation	Cover, 22 leaves, abstract cards
First printing	170 numbered copies

CONTENTS

Figures:

INTRODUCTION

In an increasingly complex world in which communication requirements (such as information transmittal between a nuclear-weapons carrier and its target) are becoming highly sophisticated, the mechanics of information-transfer are of primary concern. In 1948, Shannon (Ref. 1) related communications to mathematical formulas. For example, he likened information h to thermodynamic entropy wherein information can be shown to depend on the log of the probability P of receiving a given symbol of a defined set by

$$h = \log_2 P \tag{1}$$

However, many factors such as emotional impact can modify this clean definition for information.

In addition to the need for more refined methods of communication transfer, there is also a need for the transmission of a high density of information per communication system.

There is wide agreement that a maximum of information can be transmitted by the appropriate modulation and demodulation of electromagnetic radiation. In fact, this seems to be the only possible mechanism for use under some circumstances. Also, there is strong evidence that the higher the radiation frequency, the higher the possible density of information transmission obtainable. From a purely practical point of view, however, this latter statement has yet to be proved and there are very real limitations to the placement of a theoretical maximum of information on a radiation wave and the recovery of such information at the receiver.

Since, at present, the upper frequency limit on carrier wave modulation is four or five orders of magnitude less than the upper frequency limit on optical frequencies (which at 6328A is approximately 4.74×10^{14} sec^{-1}), it is impractical to work with modulation of carrier waves having frequencies beyond the visible in attempting to achieve a greater densification of information. This is especially true since man has vast stores of information about the visible part of the spectrum, and the advent of lasers has markedly augmented his ability to obtain greater information transmission in the visible and near visible.

This report reviews the optical characteristics of two prototype external light modulators in experimental use at NOTS and describes some of their possible applications to information transmission. The two modulators have the thin, flat, disk-shaped Fabry-Perot (F-P) interferometer design. One, which has been evaluated experimentally, uses the piezoelectric approach and the other, presently under investigation, makes use of electrooptic changes in refractive indices to control optical thickness.

THEORY

GENERAL CARRIER WAVE MODULATION FREQUENCY LIMITATIONS

Two broad classes of laser modulators have been considered historically:

1. Internal modulators for use in controlling the light intensity within the geometrical confines of the laser; e.g., possible Zeeman splitting.

2. External modulators for controlling the light intensity after the light leaves the laser proper; e.g., a mechanical shutter.

In either case, the upper frequency limit to carrier wave modulation is dependent on how often one can observe the controlled external effects (modulation) impressed on the propagating wave. For instance, for the internal modulation of a laser of optical length $n'd$, the effect of a wave which is altered or modulated at end 1 of a laser (as shown in Fig. 1) cannot be seen externally at end 2 for $n'd/c$ seconds. Thus, a meaningful upper frequency limit on such modulation is approximately $c/n'd$ sec^{-1}. For example, internal modulation of a laser 100 cm long would have an upper frequency limit of $c/100n' = 2 \times 10^8$ sec^{-1} at $n' = 1$.

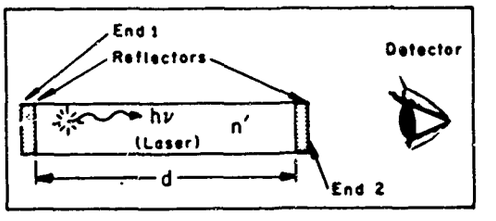

FIG. 1. Internally Modulated Laser.

External modulation, on the other hand, can be used to overcome this limitation to some extent by making use of modulation devices that are geometrically several orders of magnitude thinner than a laser in the direction of light propagation. Then, however, other phenomena such as aperture diffraction or interference-fringe-formation time become the new frequency limiting parameters.

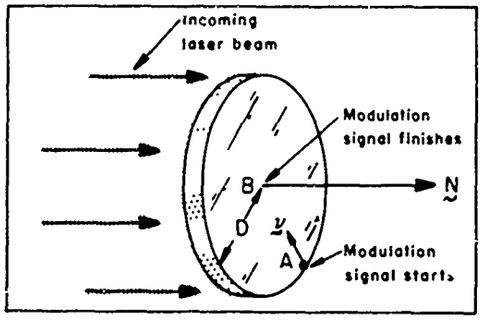

FIG. 2. Disk-Shaped External Laser Modulator.

A thin, flat external modulator with its surface normal $\underset{\sim}{N}$ parallel to the laser beam (see Fig. 2) requires that the modulating signal affect the entire beam cross section uniformly within a given time interval; the reciprocal of this time interval is approximately the upper frequency limit. For example, assuming that the modulating signal for a modulator of radius D begins on the circumference of the aperture at point A and travels at velocity v to the aperture center point B in time D/v, then the upper frequency limit is v/D. This frequency can be increased by making the aperture smaller, but this change introduces the Fraunhofer diffraction (Ref. 2, p. 395).

Taking most of these frequency limiting factors into consideration, it appears that the upper frequency limit to carrier wave modulation is about 10^{10} to 10^{11} sec^{-1} for lasers of a practical size for use in communicating over large distances in space.

FABRY-PEROT INTERFEROMETER CHARACTERISTICS

The classic F-P interferometer (Fig. 3) consists of two flat parallel surfaces, separated by optical spacing n'd.[1] Both flat surfaces will generally have high optical reflectivity which is obtained either by using heavy layers of metal (aluminum, gold, or silver), several layers of alternating high and low index of refraction dielectrics (zinc sulphide and cryolite), or a combination of metal and dielectric layers. The space surrounding the F-P has a refractive index n and the space separating the two plates has a refractive index n'.

[1]Some F-P interferometers used as laser resonators consist of two spherical reflectors of equal radius of curvature, with each reflector having the same radius of curvature.

Using Fig. 3, an electromagnetic wave incident from the material medium of index n upon surface A having an amplitude $\underset{\sim}{E}_i$, is amplitude-split into two waves--a reflected wave and a transmitted wave. For example, $r\underset{\sim}{E}_i \triangleq \underset{\sim}{E}_r$ is the fraction of $\underset{\sim}{E}_i$ reflected at surface A, and $t\underset{\sim}{E}_i \triangleq \underset{\sim}{E}_t$ is the fraction of $\underset{\sim}{E}_i$ transmitted at surface A, etc.[2]

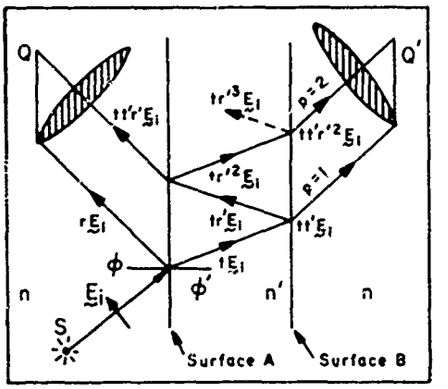

FIG. 3. Classic Fabry-Perot Interferometer.

Each of the two prototype external modulators discussed in this report is of the F-P interferometer configuration (Ref. 2), which is geometrically similar to Fig. 2. In each modulator, reflected and transmitted light intensities are controlled by fine adjustments made in one of the four highly sensitive parameters controlling the intensities (Ref. 3). Two methods of adjusting the F-P intensity are discussed below.

Piezoelectric Change in the Spacer Thickness d

The intensity modulation at Q', discussed in Appendix A and calculated by Eqs. (5) and (14), can be achieved by small variations in the spacer separation d. This variation in d has been controlled successfully by using the converse piezoelectric effect[3] in at least three configurations.

---

[2]The r value is the ratio of the reflected to the incident amplitude and t is the ratio of the transmitted to the incident amplitude of electromagnetic radiation at surface A. They are given in Fresnel's formulas (Ref. 2, pp. 38 and 620).

[3]The physical deformation of a crystal which is directly proportional to an external electric field is called the converse (or reciprocal or inverse) piezoelectric effect.

Figure 4 shows examples of two configurations of historical significance used to examine the many complex vibration modes of piezoelectric materials and as wavelength scanning interferometers (Refs. 4, 5, 6, 7, and 8). With minor modifications, these interferometers make useful light modulators. In Fig. 4a, the F-P system consists of two carefully aligned reflectors--one evaporated on a fixed mirror and the other evaporated on the piezoelectric plate. This plate could be an x-cut piece of cultured quartz with the electric field induced by voltages developed between the metal block and the evaporated reflector (necessarily metal) on the crystal. Figure 4b shows another design where the bottom reflector is merely mounted on a tube-shaped piezoelectric material which varies its length with properly applied electric fields (e.g., Oleveite piezoelectric ceramic PZT-4), see Ref. 8.

With slight technical modifications such as the use of a nearly transparent conducting block instead of the metal block shown in Fig. 4a (for example, nesa glass or a semiconductor for use with light of $h\nu$ just below the fundamental band edge), the F-P devices shown could serve to amplitude modulate the incident light. One difficulty with these systems is the need for great care in handling so as not to disrupt the quite necessary delicate alignment of the two independent reflectors.

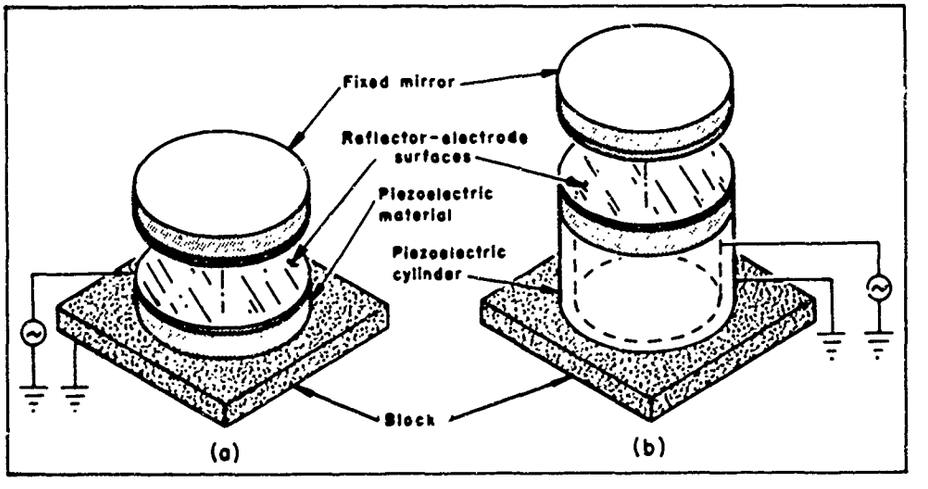

FIG. 4. Oscillating F-P Interferometers.

Electrooptic Change in the
Spacer Optical Thickness n'd

The physical dimension changes in quartz used as a spacer in piezoelectric F-P devices are, in general, accompanied by small changes in the refractive indices. The electrooptical type light modulator makes use of the changing refractive indices to control the F-P spacer optical thickness n'd, which in turn allows control of the reflected or transmitted light intensity at Q or Q' (see Fig. 3).

In all of the 20 classes of crystals that lack a center of inversion--and only in these classes (see Appendix B)--one can find both the converse piezoelectric and electrooptic electric field-induced effects. There are two independent parts to the electrooptic effect:

1. The indirect electrooptic (or piezooptic) effect is the change in the refractive index due to the changing crystal density, and

2. The so-called direct electrooptic effect is an index change which is independent of the changing crystal dimensions (Ref. 9).

For the electrooptic modulators under discussion, it is the combination of these direct and indirect effects which is significant. However, if the crystal is physically restrained from changing its dimensions by clamping, such as by applying an electric field of such a high frequency that the crystal inertia prohibits motion, only the direct electrooptic effect will exist (Ref. 10, p. 722). The piezoelectric modulator investigated was not clamped, and the wanted motion of the two F-P surfaces causing the intensity modulation was therefore accompanied by both the direct and indirect electrooptic effects. However, by aligning the electric vector of the incident linearly polarized light to be modulated in the crystallographic z-direction the combined direct and indirect electrooptic effects were cancelled out, leaving only the mechanical oscillation in the crystal thickness to induce light modulation.

BASIC THEORY BACKGROUND

Many other fundamental factors affect the development of successful laser modulators. Some of these factors are optical interference fringe formation time, the F-P characteristic curve, modulation depth limitations imposed by fringe finesse, and the interrelationships among these several parameters. These items are discussed in Appendix A.

PIEZOELECTRIC LIGHT MODULATOR

The design of the solid-etalon piezoelectric F-P laser modulator (Refs. 11, 12, and 13) investigated is shown in Fig. 5. In this configuration, the F-P spacer is a piece of x-cut[4] cultured quartz with the necessary converse piezoelectric characteristic. That is, the spacer is a solid F-P etalon completely filling the space between the reflectors. In this form, the electrodes and reflectors are simultaneously attained by the evaporation of a partially transparent metallic film on each of the two large flat surfaces. The advantage of this configuration is that once the two large surfaces are polished flat and plane-parallel, the alignment of each of the two surfaces is reasonably inert to any external force. For example, the low thermal expansion of quartz gives it temperature stability, and its rigidness and durability make it highly resistant to mechanical mistreatment.

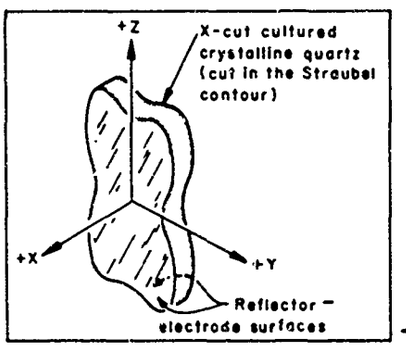

FIG. 5. Fabry-Perot Laser Modulator.

Piezoelectric Modulator Geometry

The geometry of the solid etalon interferometer is very important. With the x-cut quartz wafer, electric fields applied in the x-direction induce a near piston-like movement of the two large flat surfaces. However, since the microscopic oscillators in the quartz are tightly bound to one another (as are all molecules in solids), it is reasonable to assume that, normally, a macroscopic crystal strain in one direction will be accompanied by strain in other directions. For example, an extension in the crystallographic x-direction is usually accompanied by compression in the y-direction. These movements cause unwanted and quite complex coupled vibration modes to occur simultaneously and destroy the ideal uniform piston-like movements of the two F-P surfaces.

If, however, the x-cut wafer is shaped so that the radius in any direction in the y-z plane is proportional to the square root of Young's modulus in the radius direction, the vibration in the x-direction is a nearly uniform piston-like motion of the two large faces. Such a geometrical cut is called a Straubel contour (Ref. 14). Crystal strains, together with the dynamic nature of the refractive index, are discussed in Appendix B.

[4]The two large flat surfaces have their normals in the crystallographic x-direction.

PIEZOELECTRIC MODULATOR EXPERIMENT

Figure 6 shows the arrangement of the apparatus used in the piezoelectric laser modulator experiment (Ref. 11). The light source was a Perkin-Elmer Model 112 helium-neon gas laser operating at 6328A. Using the beam splitter, the modulated light in reflection was examined for angles of incidence near the flat surface normal. The intensity modulated signal was then deflected to an RCA #6903 photomultiplier tube, the signal from which was displayed on the lower trace of a dual-trace oscilloscope. The oscillator signal applied to the quartz was displayed simultaneously on the upper trace of the same oscilloscope so that the amplitude and phase of the oscillator and the modulated light intensity could be compared directly.

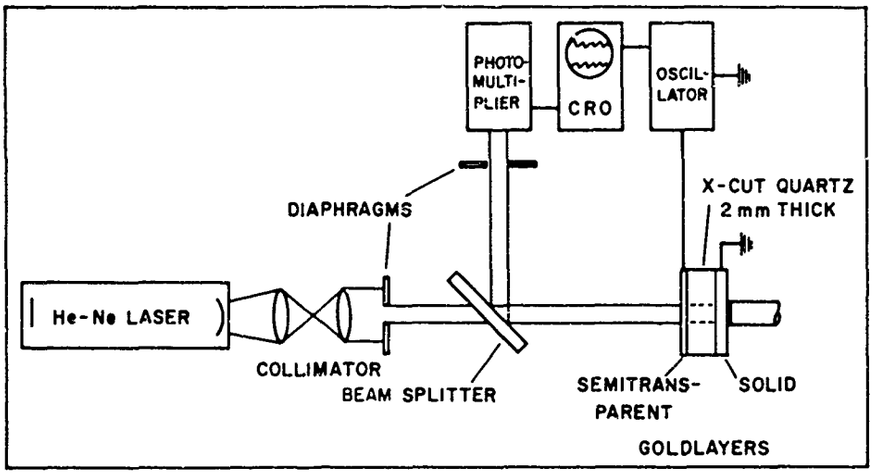

FIG. 6. Experimental Arrangement of the Piezoelectric Laser Modulator. (From "Piezoelectric Laser Modulator", by B. O. Seraphin, D. G. McCauley, and L. G. LaMarca, see Ref. 11.)

A 2mm thick wafer of cultured quartz, cut in the x-direction, was used in this apparatus. The F-P reflectors (serving as electrodes) were gold layers evaporated on both of the large flat surfaces. The reflector on the back surface was opaque and that on the front semitransparent, which necessitated the examination of the modulated intensity solely in reflection. No particular care was taken to adjust the reflectance of the front surface to achieve a large fringe finesse ($R = 60\%$ and $\mathcal{F} = 8$), see Appendix A, p. 23.

An experimentally determined portion of the reflected intensity versus phase-factor (characteristic) curve in the neighborhood of an intensity minimum is shown on the right side of Fig. 7a. The top trace on each of the three Polaroid photographs at the left in Fig. 7a shows the oscillator voltage $V_x = E_x d$ applied to the quartz electrodes; the bottom traces show the degree of intensity modulation at three locations along the characteristic curve. The point of operation on this curve can easily be adjusted by slightly varying the angle of incidence to the F-P, see Eq. (5), Appendix A. The intensity is modulated piezoelectrically from the selected point of operation.

The top photograph shows that the reflected intensity decreases for a piezoelectric change that increases the phase factor. That is, the applied oscillator voltage is out of phase with the photomultiplier signal. The bottom photograph shows that, with the point of operation on the other side of the fringe minimum, the same positive increase in phase factor gives an increase in the reflected intensity at the photomultiplier tube. That is, the applied oscillator voltage is in phase with the photomultiplier signal. The center photograph shows the modulated intensity when the point of operation is at the fringe minimum; i.e., the resultant frequency-doubling is due to the increase in the reflected intensity for both positive and negative changes in the phase factor for this point of operation.

Figure 7b is a theoretical curve of Fig. 7a and is similar to the curve shown on p. 19, Appendix A with the exception that Fig. 7b represents the reflected and not the transmitted intensity.

From Fig. 7 it is apparent that linearity in the intensity modulation is not achieved for points of operation corresponding to values of the phase factor near $2\pi m$ nor from points very far from the maximum fringe slope. The middle photograph shows an obvious nonlinearity as the piezoelectric change in δ swings down through the intensity minimum.

During this experiment, intensity modulation was observed at the fundamental 1.43 Mc/sec resonance frequency, at the second harmonic, and at several subharmonics in the range of a few hundred kc/sec. The data for Fig. 7a were taken at 167 kc/sec, one of the nonfundamental resonant frequencies where the modulation was best, instead of at the more critical high Q fundamental resonance, since the frequency stability of the oscillator used in this experiment was not adequate to hold the quartz in oscillation for any length of time. To obtain long-term modulation data at fundamental resonance, a crystal-controlled oscillator with high frequency stability is needed.

The maximum depth of modulation was approximately 22%, as determined by piezoelectrically modulating a mechanically chopped incident laser beam having a beam cross section power consumption of approximately 0.2 watts/cm^2.

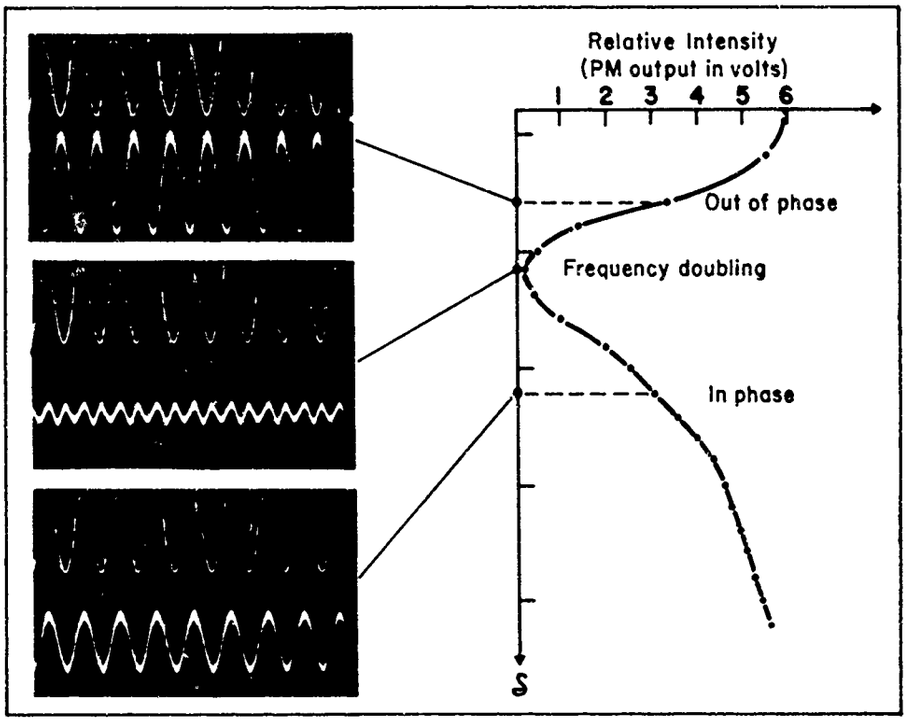

FIG. 7a. Intensity of the Light Beam Reflected From the Modulator, Measured as a Function of the Phase Factor, δ.

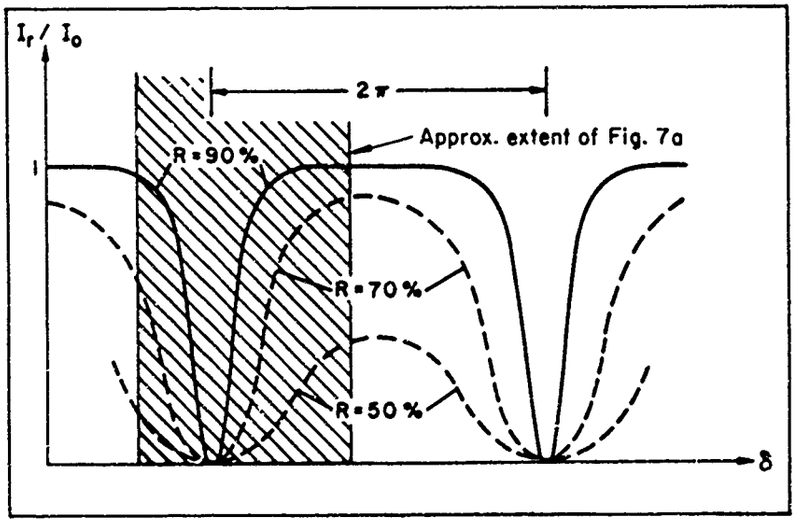

FIG. 7b. Reflection Characteristic Curve of a Fabry-Perot Interferometer as a Function of the Phase Factor.

EXPERIMENTAL INTERPRETATION

For applications in which high frequencies are not necessary, the piezoelectric laser modulator offers several advantages. Since it is essentially a mirror of variable reflectance, it has a large aperture and small light loss. In addition, the active elements are two surfaces of a durable crystal with an extremely low coefficient of thermal expansion. This results in a high degree of resettability, stability, and ruggedness. Also, for a given driving voltage, the point of operation on the characteristic curve can be controlled by varying the angle of incidence to adjust the modulation depth, the wave shape, and the reflected light level. Most importantly, perhaps, reasonable modulation depths are obtained with low power consumption per cross-sectional area of the incident beam.

However, for applications in which high frequencies are necessary, the piezoelectric laser modulator has some distinct disadvantages, some of which can be overcome fairly easily. The mechanical motion of the quartz plate heats the surrounding atmosphere which then causes slowly varying and nonuniform refractive index changes in the external optical path. This could be avoided by rapidly circulating the surrounding atmosphere, as with a fan. A better solution would be to mount the quartz in a vacuum. Since the resonance frequency is only inversely proportional to the thickness of the quartz wafer, there is a rather low upper frequency limit set by the minimum thickness to which the quartz can be polished. A thickness of 50 microns, for instance, would only give a resonance frequency of 57 Mc/sec. Even operation at higher harmonics would not provide modulation at low microwave frequencies.

ELECTROOPTIC LIGHT MODULATOR

The prototype electrooptic modulator presently under evaluation is similar in design to the solid etalon quartz device. An exploded view of the modulator is shown in Fig. 8.

The F-P geometry for this modulator is similar to that of the piezoelectric modulator with the exception of the Straubel contour. The fundamental difference between the two devices is that the potassium dihydrogen phosphate (KDP) used as the F-P spacer material in the electrooptic system (see Appendix B) depends solely on the optical-thickness change due to the refractive index dependence[5] on the externally applied electric field in the crystallographic z-direction (Fig. 9 and Refs. 15, 16, 17, 18, and 19).

[5]The mechanical strain is insignificant for high frequencies due to the crystal inertia; also the surviving piezoelectric constant d_{36} is only a shear strain constant (Appendix B).

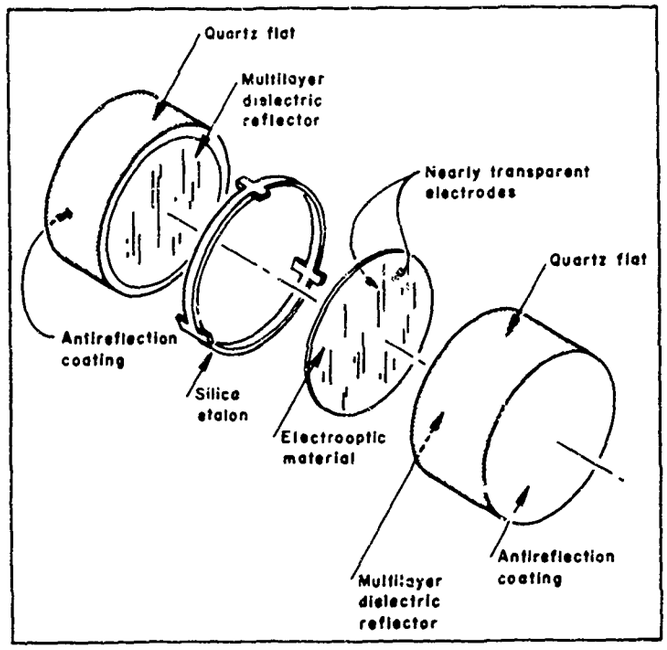

FIG. 8. Exploded View of Modified Electrooptic Laser Modulator.

With the possible exception of ruggedness and durability, this electrooptic modulator has all of the advantages of the quartz modulator. In addition, this device operates independently of any mechanical resonant frequency (above 1 Mc/sec) and the electrooptic effect shows little deviation from the clamped low-frequency effect for frequencies up to 2.5×10^{10} sec^{-1} (Ref. 20). This high frequency response is of the same order of magnitude as the F-P limitations imposed by the parameters that dictated the maximum modulation frequency curve shown in Appendix A. Therefore, the electrooptic mechanism for controlling the F-P spacer thickness with KDP imposes no additional frequency limitations beyond those discussed in Appendix A.

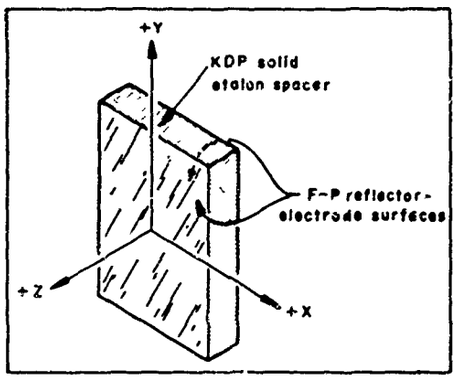

FIG. 9. Solid Etalon Electrooptic Fabry-Perot Laser Modulator.

KDP is, however, difficult to optically work-flat and plane-parallel. For this reason, the geometry of Fig. 8 is suggested instead of that shown in Fig. 9.

The two quartz flats with the multilayer dielectric reflectors are shelf items from, for example, the Perkin-Elmer or Spectra-Physics companies since the end reflectors for their helium-neon gas lasers are ideal for use with this laser modulator. These reflectors are flat to better than $\lambda/100$, have a maximum reflectivity at the gas laser wavelength, 6328A, and have the same dimensions as those of the laser-beam cross section.

One problem with any piezoelectric or electrooptic F-P system in which the reflectors are not themselves electrical conductors is that of finding transparent electrodes. Sputtered CdO has been used (Ref. 21), but it has such high resistivity that the modulating electric field is necessarily restricted to low frequencies. An alternative electrode configuration[6] which has been effective for thicker KDP wafers (d = 0.6 cm) is shown in Fig. 10.

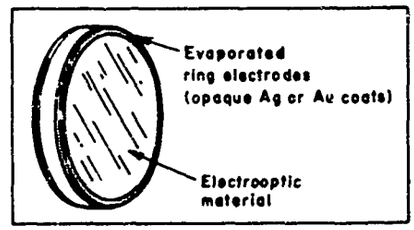

FIG. 10. Spacer With Ring Electrodes.

In this case, the ring electrodes cover only the circumferences of the electrooptic material. The electrodes, therefore, can be opaque gold or silver evaporations of low resistivity that will not obstruct the light propagation.

[6]See Ref. 22. Also, the author has varied the optical path length of one beam of a Young's double-slit experiment using a similar electrode geometry on KDP 0.635-cm thick.

CONCLUSIONS

In the previous discussion of theory and in Appendix A, it is indicated that amplitude modulation of laser light of up to 10^{10} or 10^{11} sec^{-1} is possible with the use of modified F-P interferometers. From initial investigations, it appears that the piezoelectric spacer is further limited to approximately 10^{8} sec^{-1}. In addition, since laser operation depends on the spacer vibration, the inherent mechanical ringing of piezoelectric plates causes the amplitude modulated intensity to be a poor reproduction of the modulating electrical signal. However, for low-frequency operation in which large information content is not too important, and in which mechanical ruggedness and inertness to a surrounding medium are necessary, the durable quartz spacer is an excellent choice.

The electrooptic mechanism, on the other hand, will respond to frequencies of up to 2.5×10^{10} sec^{-1} with no difficulty and its operation in the F-P does not depend on a resonance phenomenon nor mechanical vibration. One disadvantage is that none of the several highly electrooptic materials[7] are as durable as quartz. The techniques of modern packaging may, however, eliminate this disadvantage in time. Temperature stability is a problem for KDP and its deuterated cousin (see footnote 13, Appendix B, p. 35), since their electrooptic constants are highly temperature-sensitive, as shown in Fig. 11. However, when the mechanism is operated below 300°K, the electrooptic effect becomes much more effective than at 300°K. Above 300°K, the temperature-induced change in r_{63} is not significant.

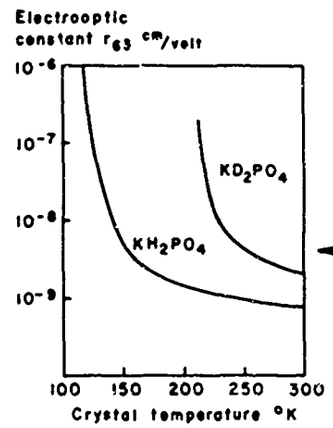

FIG. 11. Electrooptic Constant r_{63} Vs Temperature for Ordinary and Deuterated KDP.

The most serious problem which plagues any F-P modulation system today is, perhaps, that of achieving the 10^{10} sec^{-1} bandwidth. A method of placing the large bandwidth signals on the F-P device must be developed. A high frequency modulation to the incident light has been obtained in some instances (Ref. 20) by using KDP in microwave cavities to replace the F-P electrodes. However, this offers no solution to the bandwidth problem.

---

[7]For example: $NH_4H_2PO_4$, RbH_2PO_4, $NH_4H_2AsO_4$, KH_2AsO_4, CuCl, sphalerite ZnS, and GaAs.

LASER MODULATION APPLICATIONS

The laser has been around long enough now for those predicted breakthroughs in optical ranging, communications, medicine, etc. to have been realized. The fact that so much effort has produced few, if any, breakthroughs (except those achieved in basic research investigations that, for example, made use of the large electric fields inherent in the solid-state lasers) is strong evidence that few scientific innovations can advance to practical use without augmentation from work in related fields. The development of complete laser communications systems is contingent upon future technological advances in several fields of endeavor.

One specific information-transfer application for an F-P laser modulation system, such as those described in this report, might be as a passive communication link for an orbiting satellite (Fig. 12 shows this concept). Vast amounts of recorded data could be fed simultaneously to an F-P system in a satellite for transmission upon request, using the F-P setup shown in Fig. 13. The corner reflector or similar device insures that the interrogating beam and the return beam upon which the satellite data are to ride travel the same optical path--barring abrupt changes in the refractive indices of the earth's surrounding atmosphere.

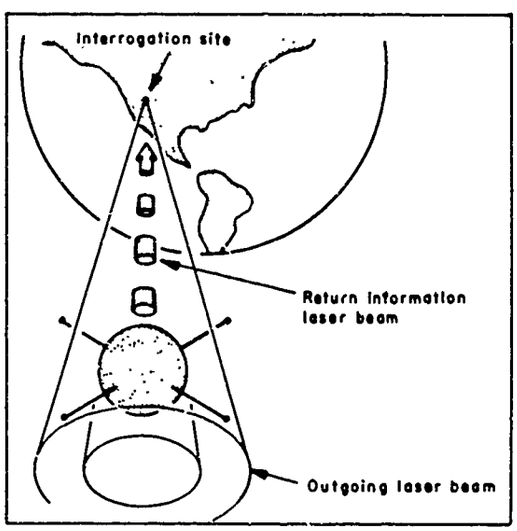

FIG. 12. Concept for a Passive Satellite Communication System.

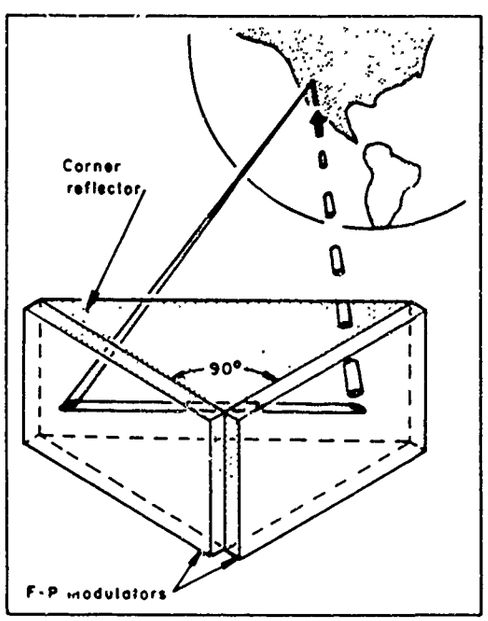

FIG. 13. Possible F-P Laser Modulator Communications Link.

Appendix A

RELATED THEORY AND BACKGROUND INFORMATION

OPTICAL INTERFERENCE

In a study of interferometer performance, optical interference becomes an important consideration. Optical interference fringes can be formed only by combining two or more electromagnetic waves having at least partial mutual coherence (Ref. 2, p. 491). Historically, the F-P interferometer has been designed to provide this coherence by the proper transformation of ordinary incoherent light.[8] Figure 14 illustrates three F-P interferometer systems.

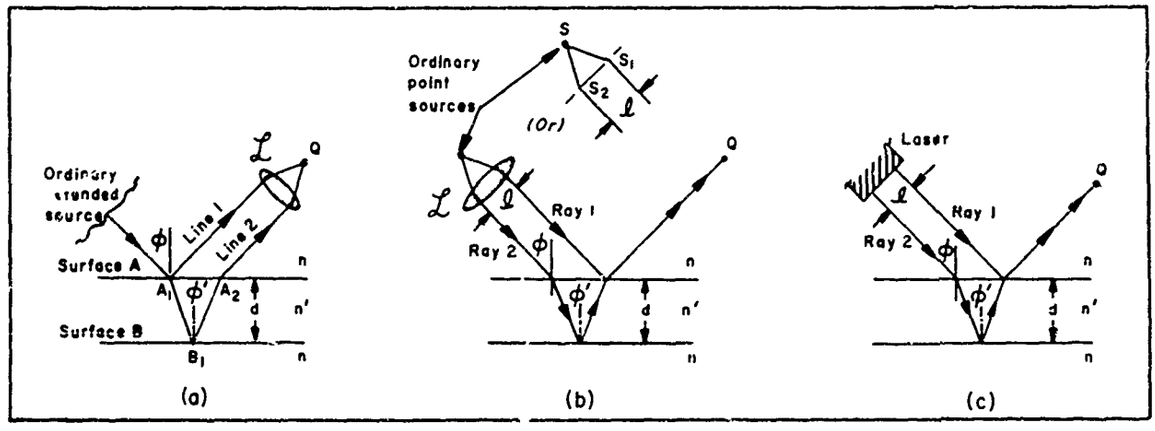

FIG. 14. Three Fabry-Perot Interferometer Systems.

In Fig. 14a, a single ray from an extended ordinary light source strikes surface A and is amplitude split. The reflected ray (ray 1) propagates along line 1 to point Q and the transmitted ray (ray 2) follows the indicated path along line 2 to point Q. The two rays obviously have some nicely ordered phase relationship with one another since they both came from a single ray. (A similar relationship exists for point Q′ in transmission.) Since the rays have different paths in leaving the F-P, except at $\phi = 0°$ or $90°$, a lens must be used to recombine them at point Q. Now, whether constructive or destructive interference takes place at point Q depends on the optical path difference between the two rays; i.e.,

[8]Partially coherent light (neglecting stimulated emission) is achieved by amplitude splitting and wavefront splitting. Devices such as Fresnel's and Lloyd's mirrors, Young's double slits (Ref. 23), and the F-P interferometers are used to achieve partial coherence.

$$\Delta\mathcal{L} = A_1 B_1 A_2 Q - A_1 Q \tag{2}$$

The path difference $\Delta\mathcal{L}$ reduces to

$$\Delta\mathcal{L} = 2n'd\cos\phi' \text{ (Ref. 2, p. 281)} \tag{3}$$

By equating the relationships for the path difference $\Delta\mathcal{L}$, measured in units of the free space wavelength λ_o, and their phase difference δ, measured in units of the wave period 2π, one finds that

$$\frac{\Delta\mathcal{L}}{\lambda_o} = \frac{\delta}{2\pi} \triangleq m \tag{4}$$

where m is defined as the order of interference.

The path difference can be expressed as a phase difference δ (where δ is called the phase factor) between any two rays at Q by substituting Eq. (3) into Eq. (4).

$$\delta = \frac{2\pi\Delta\mathcal{L}}{\lambda_o} = \frac{4\pi n'd}{\lambda_o}\cos\phi' \text{ (see footnote 9 below)} \tag{5}$$

The four highly sensitive parameters--n', d, ϕ', and λ_o--said to control the reflected and transmitted intensities from the F-P are present in Eq. (5). (ϕ and ϕ' of Figs. 3 and 14 are related by Snell's law, see Ref. 24, p. 404 and Ref. 2, p. 38 for isotropic materials. For a more general treatment, see Ch. 14 of Ref. 2.)

There are other geometries similar to Fig. 14a that produce interference using ordinary light sources (see Fig. 14b). That is, the lens can be placed between the source and the F-P, and the extended source can be replaced by a point source. Or, to go further, the lens can be completely replaced by double slits (Young's slits) having separation ℓ.

---

[9] Eq. (5) is not valid for F-Ps which have metal reflectors (Ref. 2, pp. 329 and 611). Metals absorb electromagnetic radiation and, in general, there is a phase change upon reflection which differs from π, depending on the values of the refractive indices adjoining the metal surfaces. If, however, the two metal reflectors are identical, Eq. (5) becomes $\delta = 4\pi n'd/\lambda_o \cos\phi' + 2\beta$, where β is the phase change upon internal reflection.

In the Fig. 14b configuration, the F-P serves only to recombine the two separate rays and is, therefore, quite redundant in producing interference fringes in the ordinary sense--i.e., amplitude splitting by the F-P is not needed. Also, the previously stated relationships for $\Delta\mathcal{F}$, δ, etc. are still valid. Both rays in Fig. 14b travel from the F-P along the same line toward point Q when ℓ, n', ϕ', λ_o, and d are properly chosen. Thus, the rays travel in opposite directions in the Fig. 14a and b geometries; i.e., the primary wave in Fig. 14b is split into two rays by the double slits and are recombined by the F-P, and then travel in one line to Q, while the rays in Fig. 14a travel in two lines from the F-P and are recombined at Q by the lens.

Figure 14c illustrates the direction and acceptance of the two rays when a laser is used to illuminate the F-P device. Equation (5) also holds for Fig. 14c interference, since for fixed values of n', d, and λ_o there exists the same discrete values of ϕ' for which δ will be an integral multiple of 2π. For the Fig. 14c configuration, ℓ is automatically chosen from the spatial continuum of rays, independent of the value of λ_o.

The previous paragraph points up one of the interesting characteristics of an extended, highly coherent light source such as a gas laser, and explains why, in this instance, a modulated intensity can be obtained at point Q without using lenses or similar devices. It is also apparent from Eq. (5) and Figs. 3 and 14 that the intensity at Q or Q' can truly be modulated by holding ϕ' and λ_o constant and then oscillating either n' or d.

However, in most cases, a lens will be introduced in front of the radiation detector. For example, even a direct visual detection of the F-P light involves the eye lens, which is an extremely foolish method of detecting laser radiation. But more importantly, a lens should be used at the detector to gather the maximum possible light from the distant modulator--especially when there are large modulator-detector (or transmitter-receiver) separations.

F-P CHARACTERISTIC CURVE AND RELATED TERMINOLOGY

Figure 15 shows how the light intensity transmitted through the F-P to a point Q' (see Fig. 3) varies with the phase factor δ for several values of F-P reflectivity R, where

$$R \triangleq \frac{E_r^2}{E_i^2} = r^2 = r'^2 \qquad (6)$$

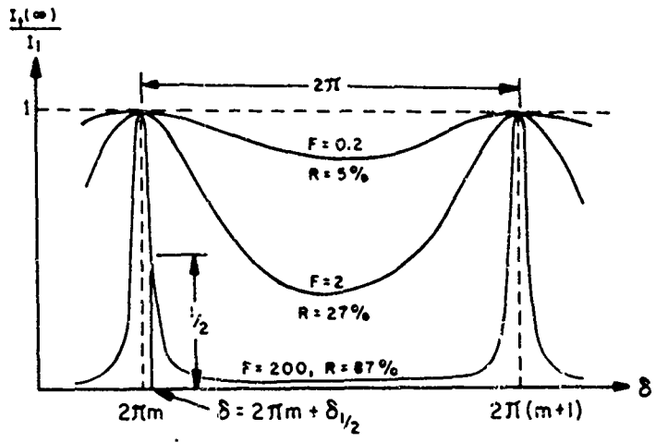

FIG. 15. Transmission Characteristic Curve for an F-P Interferometer.

The phase factor δ can be continuously increased by holding three of the highly sensitive parameters constant (e.g., n′, ø′, and λ_o) and varying the fourth, in this case, d. (The F-P reflectivity can be increased by evaporating thicker layers of metal or by increasing the number of dielectric layers deposited on the two F-P surfaces.)

The equation governing the curves in Fig. 15 comes about quite naturally (Ref. 2, p. 323). As demonstrated in Fig. 3, the combined amplitude from all of the rays transmitted through the F-P to Q′ is

$$\underset{\sim}{E}_t(p) = tt'(1 + r'^2 e^{i\delta} + \ldots + r'^{2(p-1)} e^{i(p-1)\delta})\underset{\sim}{E}_i \qquad (7)$$

where p = the number of rays.

Now, if ø′ is made small enough, the number of rays, p, which contribute to the intensity at Q′ approaches infinity, and Eq. (7) becomes

$$\underset{\sim}{E}_t(\infty) = \frac{tt'}{1 - r'^2 e^{i\delta}} \underset{\sim}{E}_i \qquad (8)$$

Further, since tt′ is defined as transmissivity T, and $r^2 = r'^2$ is defined as the reflectivity R, Eq. (8) can be written

$$\underset{\sim}{E}_t(\infty) = \frac{T}{1 - Re^{i\delta}} \underset{\sim}{E}_i \qquad (9)$$

The intensity at Q′ is given by

$$I_t(\infty) = E_t(\infty) * E_t(\infty) \tag{10}$$

which reduces to

$$I_t(\infty) = \frac{T^2}{1 + R^2 - 2R\cos\delta} I_i \tag{11}$$

Neglecting absorption, then

$$T + R = 1 \tag{12}$$

and using this relationship plus the simplifying substitution

$$F = \frac{4R}{(1 - R)^2} \tag{13}$$

Eq. (11) can be written as

$$\frac{I_t(\infty)}{I_i} = \frac{1}{1 + F\sin^2\frac{\delta}{2}} \tag{14}$$

as plotted in Fig. 15.

Finesse ($\mathcal{F}$) is defined as the ratio of the phase factor separation between adjacent peaks (or adjacent interference fringes) to the width of one such transmission peak at half maximum in units of the phase factor (see Fig. 15). The finesse is, therefore, defined as

$$\mathcal{F} = \frac{2\pi}{2\delta_{1/2}} \tag{15a}$$

Upon substitution of the value of δ from Eq. (14) which makes

$$\frac{I_t(\infty)}{I_i} = 1/2$$

for a fixed value of F and therefore R, into Eq. (15a), one finds that

$$\mathcal{F} = \frac{\pi}{2 \sin^{-1} \frac{1}{\sqrt{F}}} \tag{15b}$$

where F is given by Eq. (13). The reflectivity factor F and reflectivity R versus finesse are plotted in Figs. 16a and b.

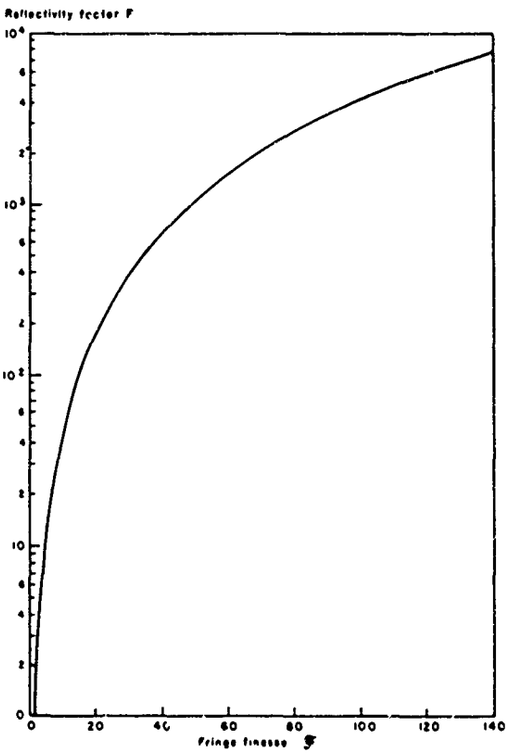

FIG. 16a. Reflectivity Factor F Vs Finesse $\mathcal{F}$.

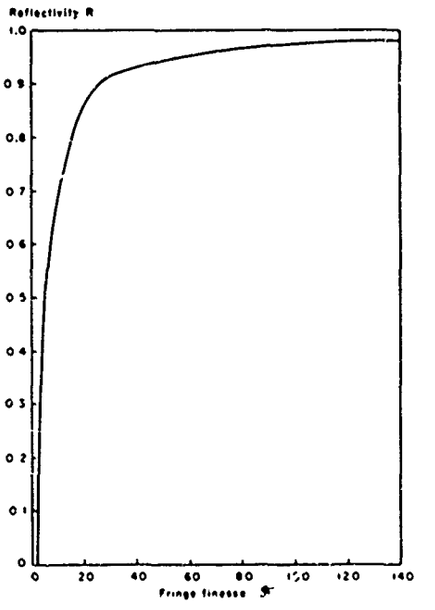

FIG. 16b. Reflectivity R Vs Finesse $\mathcal{F}$.

If $(1/\sqrt{F})^2 < 1$, then the series approximation $\sin^{-1} 1/\sqrt{F} = 1/\sqrt{F} + 1/6(1/\sqrt{F})^3 + \ldots$ holds, and when substituted into Eq. (15b) gives

$$\mathcal{F} \doteq \frac{\pi\sqrt{F}}{2} \tag{15c}$$

This is a good approximation only when $\mathcal{F} \geq 100$.

Figure 15 illustrates that, as the F-P reflectivity increases, the transmission to Q′ decreases, except in the immediate neighborhood of very critical values of the phase factor; viz., near $\delta = 2\pi m$, where m is given by Eq. (4). However, Fig. 15 is an ideal presentation that does not take into consideration the effect of F-P absorption or scattering. There is absorption that depends on the thickness of the metal or scattering that depends on dielectric coatings (still neglecting spacer absorption). Therefore, while it would seem that a transmission peak (or interference fringe) halfwidth could become infinitesimally narrow by simply increasing the reflectivity (using strictly monochromatic light and perfectly flat and parallel F-P reflectors), the absolute intensity at Q′ would become infinitesimally small. Thus, the sensitivity of any distant radiation detector will be a factor in determining a maximum practical F-P reflectivity.

The nonparallelness of any two real F-P plates adds another important but unavoidable limit to the fringe finesse. Any surface irregularity, such as a slight spherical curvature of the F-P plates, etc., places an upper limit on the finesse. For example, if the separation n′d of the F-P plates changes by λ_o/q from the center of the plates to the edge due to a spherical figure, the upper limit on the fringe finesse for this system will be $\mathcal{F}_d = q/2$--provided, of course, that the F-P plate reflectivities are high enough to give a theoretical finesse for geometrically perfect F-Ps equal to or greater than $\mathcal{F}_d$, using Eqs. (13) and (15b) (see Ref. 2, p. 332).

Modulation Depth Limitation Imposed by Finesse

Fringe finesse limits the depth of intensity modulation attainable per unit energy expended in the modulation process--whether $\mathcal{F}$ is limited by the reflectivity relationship in a system or by poor fabrication leading to a low limiting value of $\mathcal{F}_d$--since the fractional change in the intensity at Q′ depends on the halfwidth of the fringe measured in units of the phase factor δ. As shown in Figs. 17 and 18, the change in the transmitted intensity at Q′ per 5° change in the phase factor δ (i.e.,

$\Delta I(\mathcal{F},\delta) = I(\mathcal{F},2\pi m) - I(\mathcal{F},2\pi m \pm 5^\circ)$ is a function of the value of $\mathcal{F}$.[10] The highest value of $\mathcal{F}$ in Fig. 18 is $\mathcal{F} = 100$. To achieve a finesse greater than 100 for an F-P interferometer would require a fantastic piece of F-P fabrication; the F-P plates would have to be flat and parallel to $\lambda/200$.

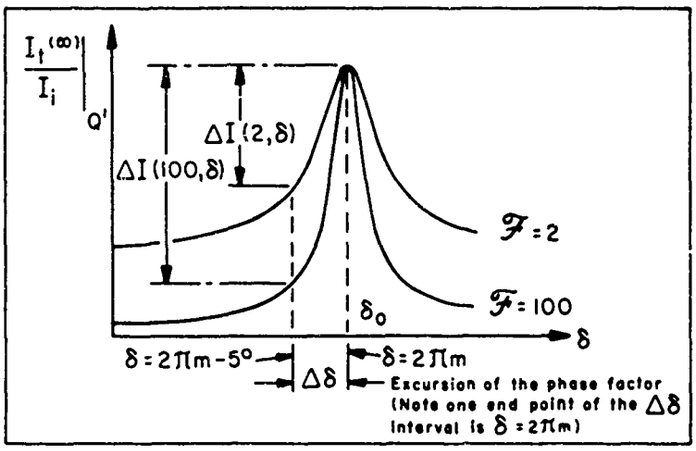

FIG. 17. Relative Intensity at Q' Vs the Phase Factor.

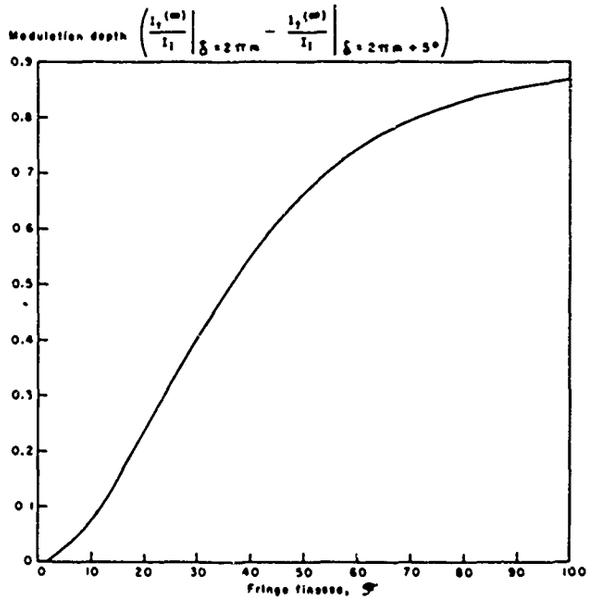

FIG. 18. Modulation Depth Vs Finesse $\mathcal{F}$.

[10] The depth of modulation for a given change in the phase factor of $\Delta\delta = 5^\circ$ is by no means a maximum when the value of $\delta = 2\pi m$ is one end point of or somewhere within the interval of $\Delta\delta$ since the rate of change of the relative intensity with respect to the phase factor is zero at $\delta = 2\pi m$ (i.e., $d[I_t(\infty)/I_i]/d\delta = 0$ at $\delta = 2\pi m$). However, for ease of calculation in this report, one end point in the $\Delta\delta$ interval was taken as $\delta = 2\pi m$.

Interrelationship of the Several Parameters

Limitations are imposed on the maximum modulation frequency by rather subtle interrelationships of the total number of rays which combine to give a relative intensity at Q′, the F-P plate reflectivities, the coherence length[11] of the radiation source being used, and the fringe finesse.

The relative amplitude at Q′ as a function of the number of rays p can be found by dividing Eq. (7) by $\underset{\sim}{E}_i$ and choosing n′, λ_o, ∅′, and d such that $\delta = 2\pi m$, where m is again the order of interference and is some positive integer 1, 2, 3 ... or zero. This gives the following expression for the maximum relative amplitude at Q′ for the p rays:

$$\frac{\underset{\sim}{E}_t(p)}{\underset{\sim}{E}_i} = tt'[1 + r'^2 + r'^4 + \ldots + r'^{2(p-1)}]$$

or

$$\frac{\underset{\sim}{E}_t(p)}{\underset{\sim}{E}_i} = tt' \sum_{n=1}^{p} r'^{2(n-1)} \tag{16}$$

Now, the following substitution can be made for the partial sum

$$S_p = 1 + r'^2 + r'^4 + \ldots + r'^{2(p-1)} \tag{17}$$

---

[11]Coherence is defined by a mutual coherence function which is dependent on temporal coherence, coherence length, coherence time, and coherence bandwidth (Ref. 2, p. 537; Refs. 21, 25, and 26). Although the coherence time is generally considered to be related to coherence bandwidth by $\Delta\tau = 1/\Delta\upsilon$, this relationship applies only to Gaussian or Lorentzian spectral distributions. Since, due to spiking, pulsed lasers seldom have Gaussian or Lorentzian distributions, their coherence time and length can be fairly well defined only by the fringe visibility function $V = (I_{max} - I_{min})/(I_{max} + I_{min})$. These intensities are formed by combining two separate light rays having velocities c and a path difference Δr. Therefore, $\Delta\tau = \Delta r/c$ can be used to give a quantitative value for coherence length Δr for any light source by choosing an acceptable but arbitrary value for V.

And this partial sum can be determined by multiplying each term of Eq. (17) by r'^2, giving

$$r'^2 S_p = r'^2 + r'^4 + r'^6 + \ldots + r'^{2p} \tag{18}$$

Subtracting Eq. (18) from Eq. (17) gives

$$S_p - r'^2 S_p = 1 - r'^{2p}$$

or

$$(1 - r'^2) S_p = 1 - r'^2$$

so that

$$S_p = \frac{1 - r'^{2p}}{1 - r'^2} \tag{19}$$

In the limit as p approaches infinity, r'^{2p} approaches zero, since $|r'| < 1$ for F-P surfaces. Thus,

$$\lim_{p \to \infty} S_p \triangleq S_\infty = \frac{1}{1 - r'^2}$$

Since the intensity at Q′ depends on the number of rays that are combined, the maximum intensity will be for $p = \infty$, and therefore a finite number, p, will result in reduced relative intensity at Q′ by the ratio

$$\frac{S_p^2}{S_\infty^2} = \left(\frac{1 - r'^{2p}}{1 - r'^2} \Big/ \frac{1}{1 - r'^2} \right)^2 = (1 - r'^{2p})^2 \tag{20}$$

or

$$\frac{I_t(p)}{I_i} = (1 - R^p)^2 \tag{21}$$

where $I_t(p)$ is the intensity at Q′ due to the superposition of the first p rays, R is the reflectivity, p is the number of rays combined at Q′, and I_i is the intensity which would exist at Q′ if the F-P were removed from between the light source and point Q′ (note that, again, absorption has been disregarded).

Now, the number of rays which will contribute at Q′ will be a function of the geometrical walk-off angle ø′. By calculating the number of rays p which would reach Q′ for any given angle ø′, the relative intensity expected can be determined by using Eq. (21). However, to achieve a maximum modulation frequency, ø′ = 0° is the optimum angle to use. In this case, the light has the shortest optical path in the F-P and, in addition, gives the ideal p = ∞.

Figure 19 shows how the maximum relative intensity at point Q′ depends on the number of rays combined. In this discussion, two values of reflectivity (82% and 97%) are assumed: For a reflectivity of approximately 82%, it takes fewer rays combined at Q′ to give a particular value of peak relative intensity than for a reflectivity of approximately 97%. For these practical values of reflectivity, these curves approach a maximum relative intensity of one quite rapidly. For example, with an F-P design limitation of $\mathcal{F}_d = 100$, a plate reflectivity below say 82% would cause the finesse to fall to less than 16 resulting in poor modulation depth for $\Delta\delta \doteq 5°$; on the other hand, a reflectivity above 97% could not improve the finesse beyond $\mathcal{F}_d$.

In addition to the dependence of the maximum relative intensity at Q′ on the number of rays p, the maximum carrier wave modulation frequency depends on p. For a single ray of amplitude E_i incident on surface A of Fig. 3 at ø′ = 0°, it takes approximately $\Delta\chi/\tilde{c}$ or $2pn'd/c$ seconds for the contribution from the first p rays to reach Q′ (neglecting the optical path external to the F-P), where $\Delta\chi$ is the path difference between the first (p = 1) ray and the last (p^{th}) ray reaching Q′. Therefore, if the intensity of each p ray is to experience approximately the same change in the parameter inducing the $\Delta\delta$ (i.e., either reflector separation d or refractive index n), the upper frequency limit will be on the order of

$$f_{up} = \frac{c}{2pn'd} \sec^{-1} \quad \text{(see Fig. 20)} \tag{22}$$

Solving Eq. (22) for p and substituting the result into Eq. (21), gives the following relationship

$$\frac{I_t(p)}{I_i} = (1 - R^{c/2n'df_{up}})^2 \tag{23}$$

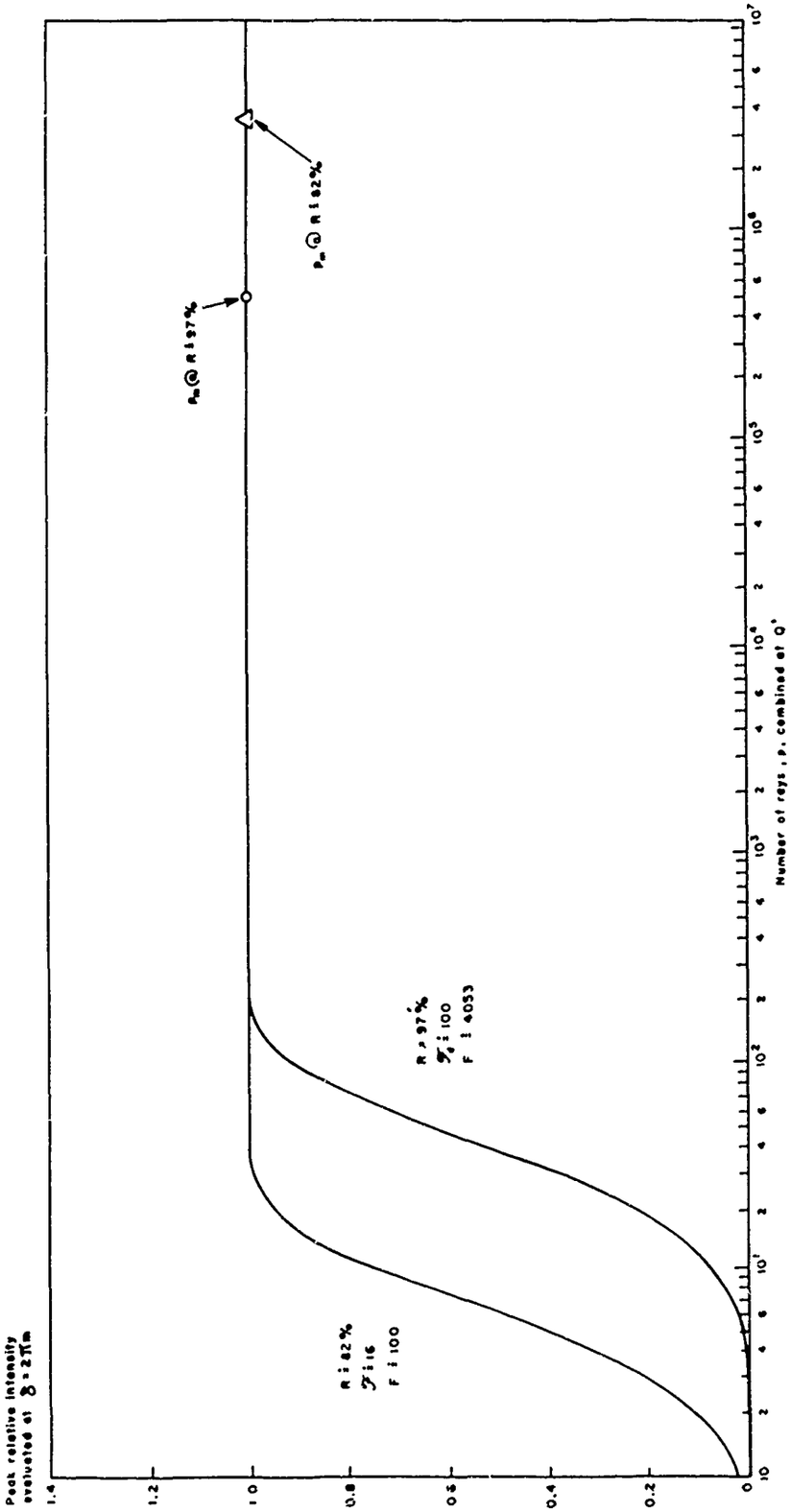

FIG. 19. Peak Relative Intensity Vs the Number of p Rays.

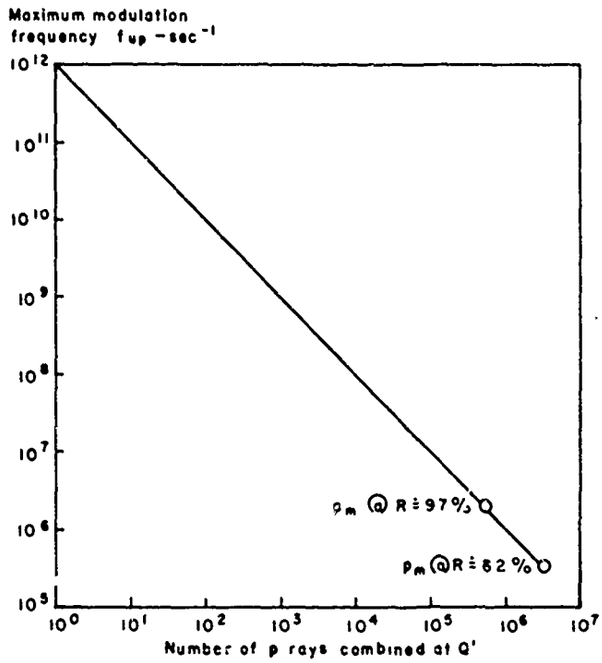

FIG. 20. Maximum Modulation Frequency Vs Number of p Rays.

Figure 21 illustrates that, with F-P devices, if carrier wave modulation of up to 5×10^9 sec^{-1} is just barely intense enough to be detected at a great distance, modulation at a higher frequency would not be detectable since the peak intensity falls off with increasing frequency.

Figures 19, 20, and 21 show some of the theoretically predicted characteristics of an F-P device illuminated by a helium-neon gas laser radiating at a central wavelength at $\bar{\lambda} = 6328$A and having a frequency spread of 20 kc or $\Delta\lambda \doteq 3 \times 10^{-7}$A. (For these calculations and Figs. 19-21, the light was assumed to have a Gaussian or Lorentzian spectral distribution, Ref. 2, p. 493 and Ref. 25, p. 12.)

The relationship of coherence length to the fringe finesse is shown by

$$\mathcal{F}\Delta\mathcal{L} \ll \frac{\bar{\lambda}^2}{\Delta\lambda} \tag{24}$$

where the right side of Eq. (24) is defined on p. 328 of Ref. 2 as the coherence length, $\mathcal{F}$ is the familiar finesse of Eq. (15), and $\Delta\mathcal{L}$ is again the total optical path difference between two rays reaching point Q'. For the combination of a gas laser source with an approximately known $\bar{\lambda}$ and $\Delta\lambda$ and an F-P with limited finesse, Eq. (24) can be used to determine the maximum value of $\Delta\mathcal{L}$ for which optical interference will take place at Q' between the first and the last so defined ray. Thus, this relationship, plus the following

$$\Delta\mathcal{L} = 2pn'd \tag{25}$$

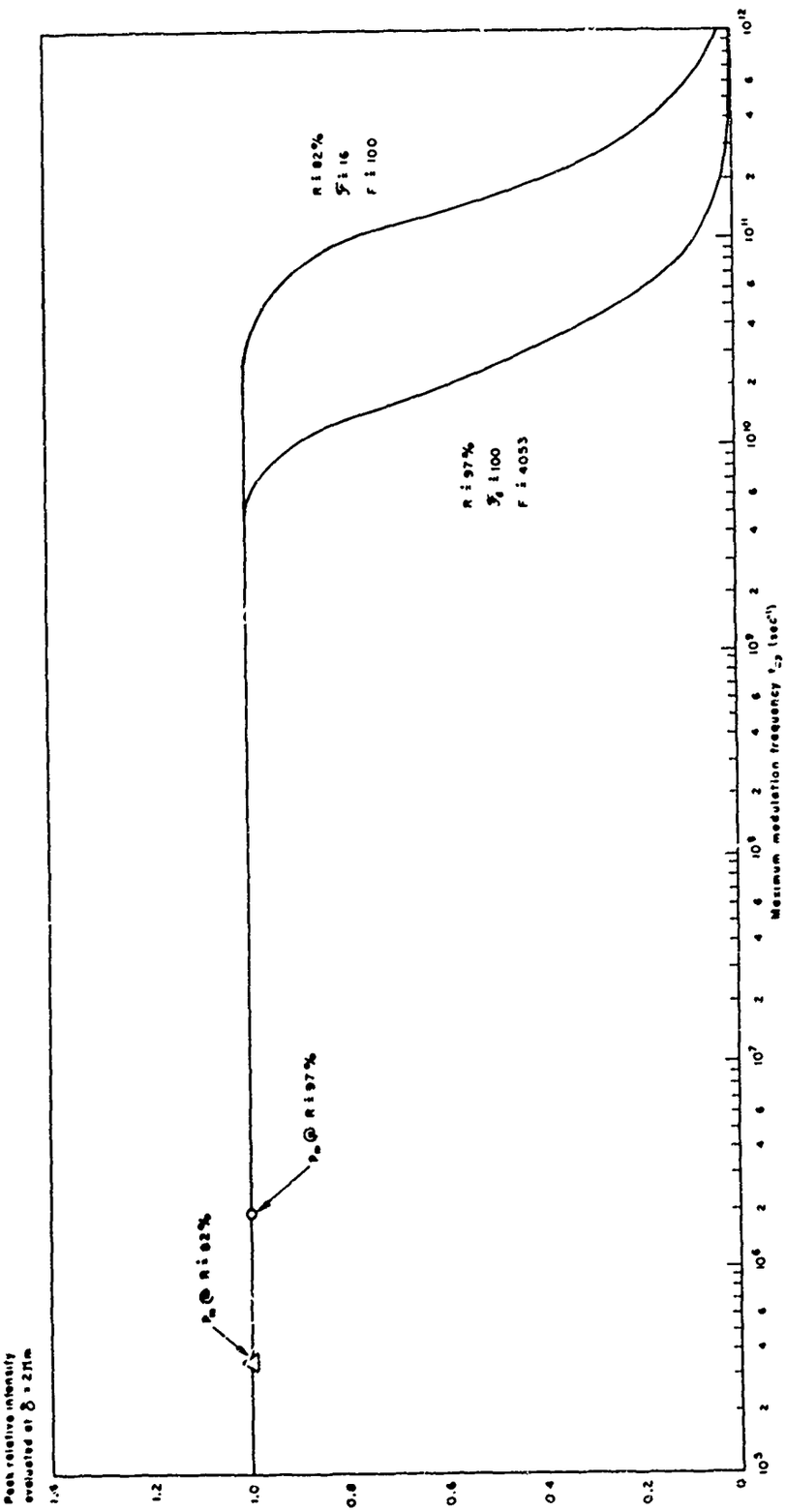

FIG. 21. Peak Relative Intensity Vs the Maximum Modulation Frequency.

gives the total path difference between the first and the p^{th} ray to reach Q′ for $\phi' = 0^\circ$ and therefore the maximum number of rays p (designated as p_m in Figs. 19, 20, and 21) which still give rise to mutual optical interference when combined at Q′. In Figs. 19, 20, and 21, p_m is marked for both values of reflectivity R and, therefore, for finesse $\mathcal{F}$.

Thus, a hypothetical F-P modulator illuminated by a helium-neon gas laser can be designed and some of its theoretical characteristics can be predicted. For example, if an application called for a maximum modulation depth (near 90%) with a minimum of energy expended in the modulation process, R should be at least 97%. This gives $\mathcal{F} \doteq 100$ as found from Fig. 16b. To obtain the highest peak relative intensity possible at the detector (consistent with the absorption and scattering), one should pick $p \geq 300$ as seen from Fig. 19. For $p \doteq 300$, the maximum modulation would be about 3.4×10^9 sec^{-1}, as shown in Fig. 20. If the modulation frequency were increased further, the peak relative intensity at Q′ would decrease as shown in Fig. 21 due to the decrease in the number of p rays that would respond to approximately the same $\Delta\delta$.

On the other hand, to communicate over a longer distance than possible at R = 97%, one might sacrifice modulation depth per unit energy expended to perhaps a low 16% (for a $\Delta\delta = 5^\circ$) and let R drop to 82%. This gives a finesse of only 16 for this 82% reflectivity as given by Fig. 16b. Then, looking at Fig. 19 for R = 82%, one needs only $p \geq 35$ to give a near maximum peak relative intensity at the distant detector. At $p \doteq 35$, the frequency of modulation can be raised to approximately 3×10^{10} sec^{-1}, as indicated in Fig. 20.

These parametric interrelationships have been presented as examples. Specific parametric combinations must be worked out for each particular problem being investigated.

Appendix B

CRYSTAL STRAINS AND INDICES OF REFRACTION

All crystals fall into one of 32 classes. Quartz is of the trigonal trapezohedral class that falls into one of the 20 categories lacking a center of inversion and having a certain one-wayness of their physical properties (Ref. 10, pp. 177 and 190; Ref. 27, p. 78). An example of the directional nature of these 20 crystal types is the strain induced when their representative crystals are subject to an external polarizing electric field (Ref. 10, p. 188; Ref. 28, p. 67).

In general, (from Ref. 10)

$$
\begin{aligned}
x_x &= d_{11} E_x + d_{21} E_y + d_{31} E_z \\
y_y &= d_{12} E_x + d_{22} E_y + d_{32} E_z \\
z_z &= d_{13} E_x + d_{23} E_y + d_{33} E_z \\
y_z &= d_{14} E_x + d_{24} E_y + d_{34} E_z \\
z_x &= d_{15} E_x + d_{25} E_y + d_{35} E_z \\
x_y &= d_{16} E_x + d_{26} E_y + d_{36} E_z
\end{aligned}
\qquad (26a)
$$

where, for example, x_x is the strain in the crystallographic x-direction, d_{ij} represents the piezoelectric constants in cm/volt, and the E_k (where $k = x$, y, or z) are the three components of the electric field. The parameters y_z, z_x, and x_y are the shear strains. For the thickness vibration of the x-cut quartz solid F-P etalon under discussion, the only contribution to the strain x_x is

$$x_x = d_{11} E_x \qquad (26b)$$

since, from crystal symmetry, d_{21} and d_{31} equal zero.

Since the light to be modulated must travel through the crystalline quartz spacer in this laser modulator under discussion, consideration must also be given to the more encompassing concept of the electric field-induced changes in the spacer optical thickness n'd and not just to changes in its physical thickness d. However, interestingly enough, the electric field which changes the quartz etalon thickness does not affect the index of refraction as seen by a light ray which is linearly polarized with its electric vector oriented parallel to the crystallographic z-axis (Ref. 10, article 534).

Even with no electric field applied, crystalline quartz is not optically isotropic but is, instead, a positive uniaxial crystal (Ref. 2, Ch. 14; Ref. 24, p. 428). That is, the velocity of light propagating in quartz is dependent on the plane of polarization--except when the ray is propagating along the crystal optic axis (crystallographic z-axis), in which case, the velocity of propagation is independent of the plane of polarization. The ordinary index of refraction controlling the velocity of rays traveling parallel to the optic axis is defined by

$$n_o = \frac{c}{v_{\parallel}} \tag{27}$$

and the extraordinary index of refraction for rays traveling perpendicular to the optic axis and having their electric vector parallel to the optic axis is defined by

$$n_e = \frac{c}{v_{\perp}} \tag{28}$$

For light penetrating crystalline quartz at arbitrary angles of incidence, the index of refraction is in general neither n_o nor n_e but is given by the equation governing Fresnel's index ellipsoid (see Fig. 22) (Ref. 2, p. 670; Ref. 24, p. 446).

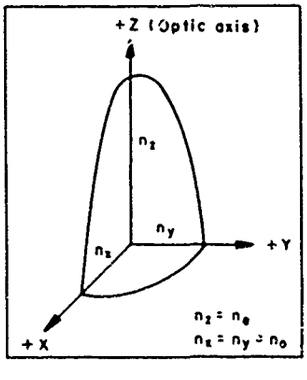

FIG. 22. Fresnel's Index Ellipsoid.

Thus, light propagating in a direction parallel to the crystallographic y-direction with its electric vector polarized parallel to the crystallographic x-axis will travel at the velocity

$$v_{y_o} = \frac{c}{n_x}$$

where the subscript y_o indicates the velocity in the y-direction associated with the ordinary index. On the other hand, if the light were to remain traveling in a direction parallel to the crystallographic y-axis with its electric vector in the crystallographic z-direction, the velocity of propagation would be

$$v_{y_e} = \frac{c}{n_z}$$

where the subscript y_e indicates the velocity in the y-direction associated with the extraordinary index of refraction.

Since quartz is a positive uniaxial crystal, n_z is greater than n_x, where n_x is equal to the ordinary index of refraction n_o, and n_z is equal to the extraordinary index of refraction n_e.

The strain in the quartz which is dependent on an applied electric field as given by Eq. (26), also affects the quartz density and, therefore, its index of refraction. The general equation which gives Fresnel's index ellipsoid for quartz as a function of the polarization of the light and the external electric field in the x-direction is given by

$$\left(\frac{1}{n_o^2} + r_{11}E_x\right)x^2 + \left(\frac{1}{n_o^2} - r_{11}E_x\right)y^2 + \frac{1}{n_e^2}z^2 + 2r_{41}E_xyz = 1 \qquad (29)$$

where x, y, and z are the principal coordinates axes when no electric field is applied, n_o and n_e are the ordinary and extraordinary indices as defined, and r_{11} and r_{41} are the sole remaining electrooptic constants after crystal symmetry conditions are considered (Ref. 29).

Equation (29) determines how the index of refraction in the x-, y-, and z-directions varies with the applied electric field, E_x. Notice that after an external electric field is applied in the x-direction, the surface described by Eq. (29) for $E_x = 0$ becomes a rotated ellipsoid having three principal axes of differing lengths (rotated because of the cross-product term for finite values of E_x). The existence of the cross-product term, which is equal to $2r_{41}E_xyz$, indicates that the choice of the old x, y, and z axes made before the field was applied is no longer the simplest one to mathematically express the new ellipsoid. On the other hand, no fixed set of coordinates would remove this electric field dependence since the directions of the principal axes move with the magnitude of this field.

Most significantly, the coefficient of z^2 in Eq. (29) is alone independent of the voltage. This means that a light ray traveling in the x-direction (as in the x-cut quartz modulator), with its electric vector plane polarized in the z-direction, will have a velocity through the quartz that is completely independent of the external electric field E_x which causes the etalon to change its physical thickness.

Just as Eq. (26a) gave the strain as a function of the applied electric field, the combined change in the indices of refraction (p. 192, Ref. 15) can be represented by[12]

$$\begin{aligned}
a_{11} - a^o_{11} &= r_{11}E_x + r_{12}E_y + r_{13}E_z \\
a_{22} - a^o_{22} &= r_{21}E_x + r_{22}E_y + r_{23}E_z \\
a_{33} - a^o_{33} &= r_{31}E_x + r_{32}E_y + r_{33}E_z \\
a_{23} - a^o_{23} &= r_{41}E_x + r_{42}E_y + r_{43}E_z \\
a_{31} - a^o_{31} &= r_{51}E_x + r_{52}E_y + r_{53}E_z \\
a_{12} - a^o_{12} &= r_{61}E_x + r_{62}E_y + r_{63}E_z
\end{aligned} \tag{30}$$

where a^o_{11}, which equals $(1/n^o_x)^2$ where the superscript zero indicates no electric field applied to the crystal; a_{11}, which equals $(1/n_x)^2$ with the electric field applied; and r_{ij} are the combined (direct and indirect) electrooptic coefficients that are analogous to the piezoelectric coefficients, d_{ij}.

Since quartz has large values for its piezoelectric constants relative to the values for its electrooptic constants, it is better known as a mechanical transducer than as an electrooptically active material. That is, for an electric field applied in the crystallographic x-direction, the piezoelectric constant $d_{11} \doteq 2.23 \times 10^{-10}$ cm/volt and the electrooptic constant $r_{11} \doteq 4.67 \times 10^{-11}$ cm/volt (Ref. 16, p. 800). On the other hand, for potassium dihydrogen phosphate (KDP), the two active constants for an external electric field applied to the crystallographic z-direction give $d_{36} \doteq 1.67 \times 10^{-9}$ cm/volt (Ref. 10, p. 209) and $r_{63} \doteq 9.0 \times 10^{-10}$ cm/volt (Ref. 30, p. 85 and Ref. 31). For this reason, distinction is often made between "piezoelectric" and "electrooptic" materials simply as a result of the historical use of the cyrstals.

[12]Normal subscript notation for matrix elements is used for the electrooptic constants of Eq. (30) while transposed notation is used for the piezoelectric constants of Eq. (26a) after Cady.

Although KDP (or KH_2PO_4), of the $\bar{4}2m$ class of the tetragonal system of crystals, is the spacer material used in the electrooptic modulator being investigated, a crystal of the class $\bar{4}3m$ of the cubic system would be equally well suited. These two crystal classes are singled out since they uniquely possess the property that allows the direction of the applied electric field and the propagation direction of the light to be modulated to be parallel during modulation. This makes the desirable large aperture F-P feature possible and permits making the F-P spacer material very thin for modulation frequency considerations. However, perhaps the most important advantage of the thin F-P structure is the resulting closely spaced electrodes. This spacing enables one to produce very high electric field strengths with comparatively small voltages; i.e.,

$$E_z = \frac{V_z}{d} \tag{31}$$

where V_z is the voltage applied to the F-P electrodes and d is the small spacer thickness in the z-direction.

Using KDP[13] as the F-P spacer material, the equation governing the Fresnel index ellipsoid, analogous to Eq. (29) for quartz, is given by

$$\frac{1}{n_o^2}(x^2 + y^2) + \frac{1}{n_e^2} z^2 + 2r_{63} E_z xy = 1 \tag{32}$$

where, as before, n_o (which equals n_x and n_y) is the ordinary refractive index that determines the velocity of linearly polarized light having its electric vector in the crystallographic x- and y-directions, n_e (or n_z) is the refractive index which determines the velocity of linearly polarized light having its electric vector in the crystallographic z-direction, and r_{63} is the sole remaining electrooptic constant for an external electric field in the z-direction after crystal symmetry is considered.

[13] If the hydrogen in KDP (KH_2PO_4) is replaced by deuterium, the potassium dihydrogen phosphate becomes potassium dideuterium phosphate (KD*P). The latter compound is significantly more electrooptic; i.e., at 300°K $r_{63} \doteq 9 \times 10^{-10}$ cm/volt for KH_2PO_4, while $r_{63} \doteq 3 \times 10^{-9}$ cm/volt for KD_2PO_4 (Ref. 30, p. 85).

Examining Eq. (32) as was done for Eq. (29), one finds that, for $E_z = 0$, it describes an ellipsoid of revolution about the z-axis. Since the ordinary index of refraction for KDP is greater than the extraordinary (i.e., $n_o = 1.5095$ and $n_e = 1.4684$ (Ref. 32) for $\lambda = 5893$A), the index ellipsoid is shaped as in Fig. 23, and further the refractive indices in the x-, y-, and z-directions are independent of the electric field applied in the z-direction. The dimensions in the figure are greatly exaggerated to show relationships.

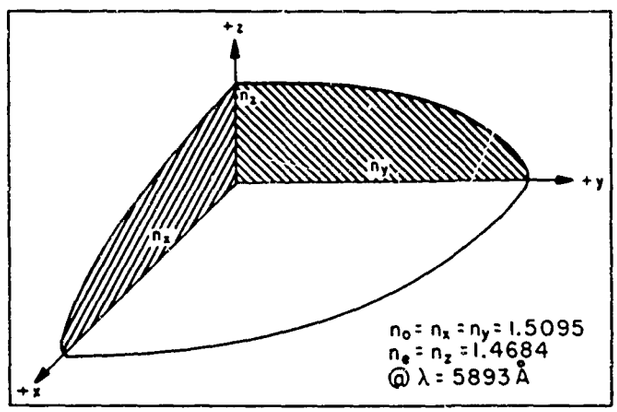

FIG. 23. Fresnel's Index Ellipsoid for KDP.

However, the cross-product term shows that there is an index change elsewhere in the x-y plane. The refractive index in the x-y plane before and after the electric field is applied in the z direction is illustrated in Fig. 24. Before the application of E_z, the cross section of the index ellipsoid in the x-y plane is a circle of radius n_o; after E_z is applied, the circle becomes an ellipse with its major x′ and its minor y′ axes at 45° to the crystallographic x and y axes. The change in the index of refraction along the two new principal x′ and y′ axes versus E_z is

$$\Delta n = \frac{1}{2} n_o^3 r_{63} E_z \tag{33}$$

This gives the indices of refraction along the primed axes as a function of E_z as

$$n_{x'} = n_o + \frac{1}{2} n_o^3 r_{63} E_z$$

$$n_{y'} = n_o - \frac{1}{2} n_o^3 r_{63} E_z \tag{34}$$

$$n_{z'} = n_z = n_e$$

where the index in the z′-direction does not change with the applied field.

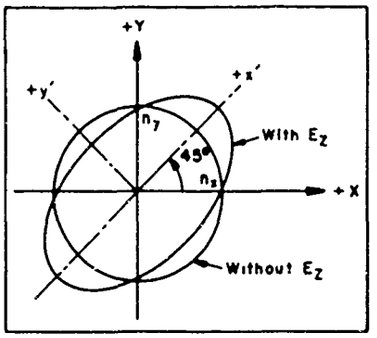

FIG. 24. Fresnel's Index Ellipsoid x-y Plane Cross Section.

Equation (33) is used to calculate the total refractive index change expected during any one complete cycle of the electric field for linearly polarized light having its electric vector along the x′ axis of the KDP, and to then determine a probable value of $\Delta\delta$ from the differential of Eq. (5). Thus,

$$\Delta n = 0.000031$$

where

$$r_{63} = 9 \times 10^{-10} \text{ cm/volt at } 300^{\circ}\text{K}$$

$$n_o = 1.5095 \text{ at } \lambda = 5893 \text{ Å}$$

$$d = 0.01 \text{ cm}$$

$$E_z = 2 \times 10^4 \text{ or } V_z = 200 \text{ volts}$$

Since the Δn only gives the index change for half the voltage cycle, the total $\Delta n_t = 2\Delta n$, or

$$\Delta n_t = 6.2 \times 10^{-5}$$

Taking the differential of Eq. (5) gives

$$\Delta\delta = \frac{4\pi d}{\lambda_o} \Delta n \qquad (35)$$

where

$$\lambda_o = 6.328 \times 10^{-5} \text{cm and } \phi' = 0^\circ$$

Substituting the proper values into Eq. (35) gives

$$\Delta\delta \doteq 7^\circ$$

which is adequate swing of the phase factor to give better than 50% modulation depth for an F-P device having a finesse of 50 or so (see Fig. 18).

REFERENCES

1. Shannon, C. E. "A Mathematical Theory of Communication," BELL SYSTEM TECH J, Vol. XXVII, No. 3 (July 1948), pp. 379-656.

2. Born, M. and E. Wolf. Principles of Optics. New York, The Macmillan Company, 1964.

3. Seraphin, B. O. and D. G. McCauley. "Low Power Light Modulators," OPT SOC AM J, Vol. LIII, No. 4 (June 1963), p. 523.

4. Dye, D. W. "Piezoelectric Quartz Resonator and Equivalent Electrical Circuit," PHYS SOC LONDON, PROC, Vol. XXXVIII (1926), pp. 399-458.

5. Straubel, H. "Modes of Vibration of Piezoelectric Crystals," PHYS ZEITS, Vol. XXXIV (1933), pp. 894-896.

6. Straubel, H. "Temperature Coefficient, Mode of Vibration, and Amplitude Piezoelectric Oscillators," PHYS ZEITS, Vol. XXXV (1934), pp. 179-181.

7. Strong, J. A. "New Method of Investigating the Modes of Vibration of Quartz Crystals," NATURE, Vol. CXXIX (1932), p. 59.

8. Mielenz, K. D. "Fringe Pattern of an Oscillating Fabry-Perot Interferometer," NATL BUR STANDARDS, J RES, Vol. LXVIII-C, No. 2 (April-June 1964), pp. 73-81.

9. Pockels, F. "On the Effect of an Electrostatic Field on the Optical Behavior of Piezoelectric Crystals," ABH GOTT, Vol. XXXIX (1894), pp. 1-204.

10. Cady, W. G. Piezoelectricity. New York, McGraw-Hill, 1946.

11. Seraphin, B. O., D. G. McCauley, and L. G. LaMarca. "Piezoelectric Laser Modulators," in the Proceedings of the Symposium on Optical Masers, ed. by Jerome Fox. Brooklyn, Polytechnic Press, 1963.

12. Johnson, L. F. and D. Kahng. "Piezoelectric Optical-Maser Modulator," J APPL PHYS, Vol. XXXIII, No. 12 (December 1962), pp. 3440-43.

13. Tolansky, S. and W. Bardsley. "Application of Multiple-Beam Interferometry to the Study of Oscillating Quartz Crystals," NATURE, Vol. CLX, No. 4102 (June 12, 1948), p. 925.

14. Straubel, H. "Oscillation Form and Temperature Coefficient of Quartz Oscillators," PHYS ZEITS HFR, Vol. XXXVIII (1931), pp. 14-27.

15. "Crystal Optics: Diffraction," in Encyclopedia of Physics, ed. by S. Flugge. Berlin, Springer-Verlag, 1961. Vol. XXV, Part I, pp. 191-198.

16. Billings, B. H. "The Electrooptic Effect in Uniaxial Crystals of the Type XH_2PO_4, Part I Theoretical," OPT SOC AM J, Vol. XXXIX, No. 10 (October 1949), pp. 797-801.

17. ------. "The Electrooptic Effect in Uniaxial Crystals of the Type XH_2PO_4, Part II Experimental," OPT SOC AM J, Vol. XXXIX, No. 10 (October 1949), pp. 802-808.

18. Carpenter, R. O'B. "The Electrooptic Effect in Uniaxial Crystals of the Dihydrogen Phosphate Type, Part III Measurement of Coefficients," OPT SOC AM J, Vol. XL, No. 4 (April 1950), pp. 225-229.

19. Billings, B. H. "The Electrooptic Effect in Uniaxial Crystals of the Dihydrogen Phosphate (XH_2PO_4) Type, Part IV Angular Field of the Electrooptic Shutter," OPT SOC AM J, Vol. XLII, No. 1 (January 1952), pp. 12-20.

20. Kaminow, I. P. "Microwave Modulation of the Electrooptic Effect in KH_2PO_4," PHYS REV LTR, Vol. VI, No. 10 (May 15, 1961), pp. 528-30.

21. Seraphin, B. O. and L. G. LaMarca. "Interferometric Study of the Electro-Optical Effect in KD*P," presented at the American Physical Society, 28-30 August 1963.

22. Strong, C. L. "How an Electric Field Can Modulate Light by Changing the Refractivity of a Crystal," SCI AM (1962), pp. 156-66.

23. Young, T. "The Interference of Light," in Great Experiments in Physics, ed. by Morris H. Shamos. New York, Henry Holt & Company, 1960.

24. Andrews, C. L. Optics of the Electromagnetic Spectrum. Englewood Cliffs, N. J., Prentice-Hall, Inc., 1960.

25. Ohio State University Research Foundation. A Discussion of Partial Coherence as Related to Optical Masers, by W. S. C. Chang and J. W. Gray. Columbus, Ohio, 1 May 1963. (Report 1579-2).

26. Mandel, L. and E. Wolf. "The Measures of Bandwidth and Coherence Time in Optics," PHYS SOC LONDON, PROC, Vol. LXXX (1962), pp. 894-897.

27. Mason, W. P. Piezoelectric Crystals and Their Application to Ultrasonics. New York, Van Nostrand, 1950.

28. Band, W. Introduction to Mathematical Physics. New York, Van Nostrand, 1959.

29. Vlokh, O. G. and I. S. Zheludev. "Changes in the Optical Parameters of Crystals Caused by Electric Fields (The Linear Electrooptic Effect)," translated from Kristallographfiya, Vol. V, No. 3 (May-June 1960), pp. 390-402.

30. Jona, F. and G. Shirane. Ferroelectric Crystals. New York, The Macmillan Company, 1962.

31. Mason, W. P. "The Elastic, Piezoelectric, and Dielectric Constants of Potassium Dihydrogen Phosphate and Ammonium Dihydrogen Phosphate," PHYS REV, Vol. LXIX, Nos. 5 & 6 (March 1 & 15, 1946), pp. 173-94.

32. Clevite Corporation, Electronic Research Division. Reference Data on Linear Electro-Optic Effects in KH_2PO_4 Type Crystals, by W. R. Cook, Jr. and H. Jaffe. Cleveland, Ohio, 15 October 1962. (Engineering Memorandum 62-24).